JACS
JOURNAL OF THE AMERICAN CHEMICAL SOCIETY

Article

pubs.acs.org/JACS

Polymer–Metal–Organic Frameworks (polyMOFs) as Water Tolerant Materials for Selective Carbon Dioxide Separations

Zhenjie Zhang,[†] Ha Thi Hoang Nguyen,[‡] Stephen A. Miller,[‡] Ann M. Ploskonka,[§] Jared B. DeCoste,[§,∥] and Seth M. Cohen*[,†]

[†]Department of Chemistry and Biochemistry, University of California, San Diego, La Jolla, California 92093, United States

[‡]The George and Josephine Butler Laboratory for Polymer Research, Department of Chemistry, University of Florida, Gainesville, Florida 32611, United States

[§]Leidos, Inc., P.O. Box 68, Edgewood Chemical Biological Center, Aberdeen Proving Ground, Maryland 21010, United States

[∥]Edgewood Chemical Biological Center, U.S. Army Research, Development, and Engineering Command, 5183 Blackhawk Road, Aberdeen Proving Ground, Maryland 21010, United States

Supporting Information

ABSTRACT: Recently, polymer–metal–organic frameworks (polyMOFs) were reported as a new class of hybrid porous materials that combine advantages of both organic polymers and crystalline MOFs. Herein, we report a bridging coligand strategy to prepare new types of polyMOFs, demonstrating that polyMOFs are compatible with additional MOF architectures besides that of the earlier reported IRMOF-1 type polyMOF. Gas sorption studies revealed that these polyMOF materials exhibited relatively high CO_2 sorption but very low N_2 sorption, making them promising materials for CO_2/N_2 separations. Moreover, these polyMOFs demonstrated exceptional water stability attributed to the hydrophobicity of polymer ligands as well as the cross-linking of the polymer chains within the MOF.

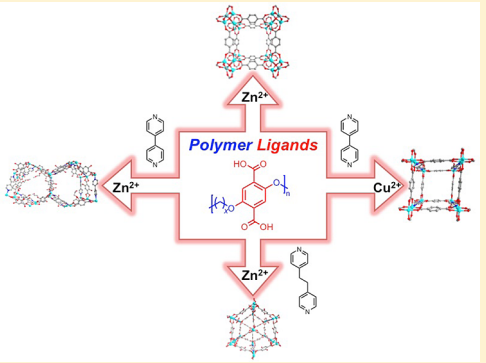

INTRODUCTION

Metallopolymer materials have received increasing attention due to their properties as stimulus-responsive,[1] self-healing,[2] conductive,[3,4] photo- and electroluminescence,[5,6] catalysis,[7] and drug delivery materials.[8,9] To the best of our knowledge, most metallopolymer materials are amorphous due to the high flexibility and random conformation of the polymer chains.[10] Synthesis of highly crystalline metallopolymers is challenging, but recently polymer–metal–organic frameworks (polyMOFs) have been reported as a new class of hybrid metallopolymer material that combines features of both organic polymers and crystalline MOFs.[11] Amorphous, linear, and nonporous polymer ligands were shown to coordinate with metal ions to form highly crystalline, three-dimensional, porous framework materials. From a synthesis perspective, this approach upends conventional wisdom in both polymer and MOF chemistry, as linear polymers are not easily organized into three-dimensional, crystalline solids, and MOFs are not readily prepared from long, flexible ligands. polyMOFs show the potential to harness not only the advantages of polymers, such as the facile fabrication of films, good processability, and chemical stability, but also the best traits of MOFs, including crystallinity, well-determined structures, and permanent porosity. Some related polymer-MOF hybrid materials have been prepared, via postsynthetic modification (PSM), whereby chemical cross-linking of the MOF is achieved through the organic ligands to form polymeric monoliths.[12−14] Other hybrids of polymers and MOFs have been described where polymerization of polymer chains is performed inside the channels of MOFs.[15−17] However, to date, only one report of polymer-derived polyMOFs has been described, wherein only analogues of the canonical IRMOF-1 (a.k.a. MOF-5) were obtained from polyether polymer ligands (pbdc-*x*a, pbdc = poly(1,4-benzenedicarboxylate), Chart 1) that contain 1,4-benzenedicarboxylic acid (H_2bdc) units as part of the polymer backbone.[11] This initial study provided insight into the factors that dictate polyMOF formation and clues that other MOF architectures might be suitable for polyMOFs.

Substituted H_2bdc derivatives have long been employed to prepare MOFs with various network structures.[18−20] In addition to IRMOF-1 ($[Zn_4O(bdc)_3]_n$), mixed-ligand systems such as pillared square grid MOFs, including $[Zn_2(bdc)_2(dabco)]_n$ (dabco = 1,4-diazabicyclo[2.2.2]octane, Chart 1) and $[Zn_2(bdc)_2(bpy)]_n$ (bpy = 4,4′-bipyridine), have been widely investigated as well.[21,22] Fischer et al. reported a honeycomb-like network (**1**) with a formula of $[Zn_2(BME\text{-}bdc)_2(bpy)]]_n$ (BME-bdc = 2,5-bis(2-methoxyethoxy)-1,4-benzenedicarboxylate, Chart 1).[23] In MOF **1**, BME-bdc and bpy linkers cross-link the Zn(II)-carboxylate secondary-building unit (SBU) chains to form a three-dimensional structure with

Received: October 21, 2015
Published: December 28, 2015

DOI: 10.1021/jacs.5b11034
J. Am. Chem. Soc. 2016, 138, 920−925

Chart 1. Ligands Used in This Work[a]

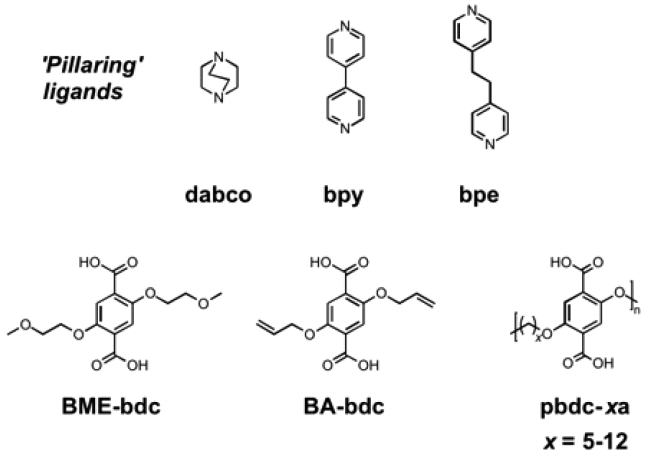

[a]"Pillaring" nitrogen-based ligands are shown in the top row. Polymer ligands (pbdc-xa) are shown in the bottom row along with monomeric carboxylate ligands.

honeycomb-like channels (Figure 1). It is noteworthy that MOF **1** exhibited selective uptake for CO_2 vs N_2 and CO_2 vs

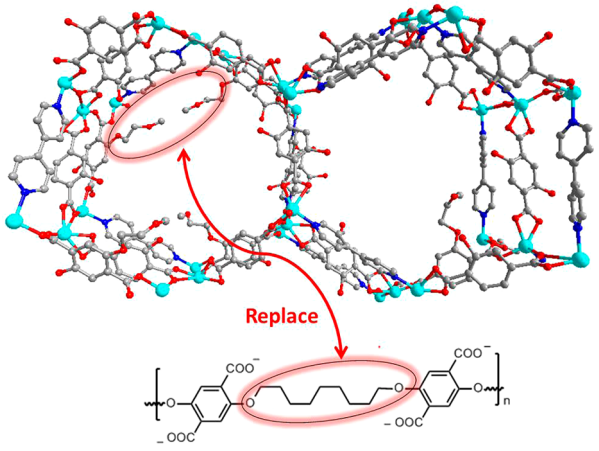

Figure 1. Packing diagram of MOF **1** along the *c*-axis direction (top); design concept for creating a polyMOF analogue of MOF **1** via replacing dangling groups by polymer chains (bottom).

CH_4. However, the instability of MOF **1** toward water hindered further studies. It was predicted by Fischer et al. that water-stable, isoreticular derivatives of MOF **1** would be promising for applications in CO_2 capture from flue gas or upgrading natural gas through CO_2 vs CH_4 separations.

The prior report on polyMOFs suggested that the water stability of polyMOFs is substantially enhanced relative to the parent MOFs via inherited hydrophobicity from the organic polymer ligands. A close examination of MOF **1** (Figure 1) indicates that the flexible $CH_3OC_2H_4-$ chains dangling from the BME-bdc linkers point into the pore channels. Therefore, a potential approach to water-stable derivatives of MOF **1** would be to tether H_2bdc moieties together across the pore space with polymer chains to form polyMOF analogues. In addition to the induced hydrophobicity from polymers, cross-linking by the polymer chains could provide additional connectivity to the framework thereby enhancing the MOF stability. However, no polyMOF analogue of MOF **1** has been reported, nor has a polyMOF with a coligand (e.g., bpy) ever been described.

RESULTS AND DISCUSSION

To examine whether polymer ligands could be used to prepare a polyMOF of MOF **1**, a series of linear, flexible, chain polymer–ligands (pbdc-*x*a, x = 9–12) were prepared via a slightly modified procedure from that previously reported.[11] Both ^{1}H and ^{13}C NMR verified the composition of the polymers (Figures S1–S8). The molecular weight values of the polymers were determined by using gel permeation chromatography (GPC) on three independently prepared samples. The polymer ligands possessed M_n values (number-average molecular weight) ranging from 5000 to 7500 g/mol, M_w values (weight-average molecular weight) ranging from 14 200 to 25 000 g/mol, and polydispersity index values (PDI) ranging from ~2.8 to 3.3 (Table 1, Figure S10). The average degree of

Table 1. Thermal, Molecular Weight, and Contact Angle (Water) Data for New Polymer Ligands

ligands	T_g (°C)	T_m (°C)	M_w (g/mol)	M_n (g/mol)	*DP*	PDI	contact angle (deg)
pbdc-9a	74	167	14 200	5000	16	2.8	113 ± 2
pbdc-10a	72	191	22 300	6800	20	3.3	110 ± 1
pbdc-11a	67	164	25 000	7500	21	3.3	114 ± 1
pbdc-12a	63	164	21 300	6700	19	3.2	120 ± 2

polymerization ($DP = M_n/(\text{F.W.}_{\text{repeat unit}})$) ranged from 16 to 21. The glass transition temperature (T_g) of the polymer–ligands decreased from 74 to 63 °C with an increasing number of methylene spacers (x = 9–12) between the H_2bdc groups in the polymer backbone (Table 1). This is consistent with previous observations that more methylene spacers increase the conformational freedom of the polymer and dilute its polar fraction, resulting in lower T_g values.[11]

As described by Fischer et al., MOF **1** is a versatile platform in which various dangling groups (e.g., methoxyethoxy, methyl, ethyl, and propyl) can be installed on the bdc moieties. Besides those reported bdc derivatives, we found that 2,5-bis(allyloxy)-1,4-benzenedicarboxylic acid,[22] BA-bdc (Chart 1), can form the isostructural MOF **1**′ as verified by PXRD (Figure 2). MOF **1**′ was used as a non-polyMOF (i.e., simple molecular ligand) "standard" for comparative studies described below.

Following the same synthesis protocol as MOF **1**, pbdc-*x*a (x = 5–12) polymer ligands were examined for their ability to form crystalline polyMOFs analogous to **1**. Powder X-ray diffraction (PXRD) patterns (Figure S10) revealed that pbdc-5a, -6a, -7a, -10a, and -11a produced mostly amorphous materials with broad peaks centered at $2\theta \approx 22°$. However,

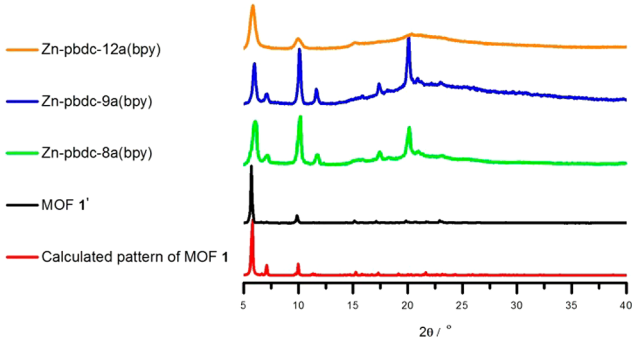

Figure 2. PXRD patterns of Zn-pbdc-8a(bpy), -9a(bpy), -12a(bpy), MOF **1**′ (prepared from BA-bdc), and a calculated pattern for MOF **1**.

DOI: 10.1021/jacs.5b11034
J. Am. Chem. Soc. 2016, 138, 920–925

PXRD data (Figure 2) revealed that pbdc-8a and -9a generated the desired products with patterns that were broad, but consistent with those of MOF **1**. Scanning electron microscopy (SEM) was employed to study the morphology and particle size of new materials. The products of pbdc-5a, -6a, -7a, -10a, and -11a exhibited irregularly shaped solids (Figures S11–S15), consistent with the PXRD pattern indicating largely amorphous materials. As shown in Figure 3a and 3c, both Zn-pbdc-8a(bpy)

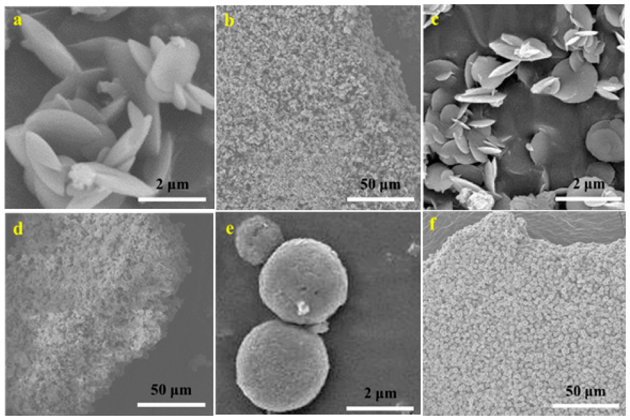

Figure 3. SEM images of Zn-pbdc-8a(bpy) (a and b); Zn-pbdc-9a(bpy) (c and d); Zn-pbdc-12a(bpy) (e and f).

and Zn-pbdc-9a(bpy) exhibit regular plate-like particles with a size of ~1–3 μm. Interestingly, the small plate-like particles were found to pack into uniform films (Figure 3b and 3d). It is noteworthy that pbdc-12 also produced a crystalline phase; however, some PXRD reflections (e.g., 2θ = 4.2° and 11.6°) were absent (Figure 2) from the expected pattern based on MOF **1**. This suggests that Zn-pbdc-12a(bpy) may exhibit a related, but not identical, structure to MOF **1**. As shown in Figure 3e, Zn-pbdc-12a(bpy) possesses distinctively spherical particles, which can also pack tightly to form uniform films (Figure 3f).

The successful preparation of polyMOFs from bpy and pbdc-*x*a inspired us to explore whether other "pillaring" linkers, such as dabco and 1,2-bis(4-pyridyl)ethane (bpe), could also form polyMOFs. Following reported procedures,[22] reactions of dabco, pbdc-*x*a, and $Zn(NO_3)_2{\cdot}6H_2O$ in a 1:2:2 stoichiometry did not afford the expected MOF products, ($[Zn_2(bdc)_2(dabco)]_n$), instead forming IRMOF materials (which do not incorporate the pillar) or amorphous materials (Figure S16). This result can be ascribed to the spatial match limitation in the $[Zn_2(bdc)_2(dabco)]_n$ structure. An examination of the $[Zn_2(bdc)_2(dabco)]_n$ structure found the nominal distance between the adjacent bdc moieties is ~7.4 Å (carbon–carbon distance, Figure S17). However, among all of the pbdc-*x*a (x = 5–12) ligands prepared, the shortest bdc distance is ~7.8 Å for pbdc-5a, which is longer than the bdc-bdc distance in $[Zn_2(bdc)_2(dabco)]_n$. This suggests a size mismatch can account for the inability of these polyMOF analogues to form.

The apparent length mismatch prompted us to try a longer coligand linker, bpe, which might better accommodate the alkane spacers in pbdc-*x*a. Reactions of bpe, pbdc-*x*a (x = 7–12), and $Zn(NO_3)_2{\cdot}6H_2O$ with a 1:2:2 stoichiometry in DMF at 120 °C afforded light yellow powders. PXRD patterns revealed that all products exhibited an unknown crystalline phase (Figure 4). The morphology and particle size of the resulting materials were determined by SEM (Figure 5). As

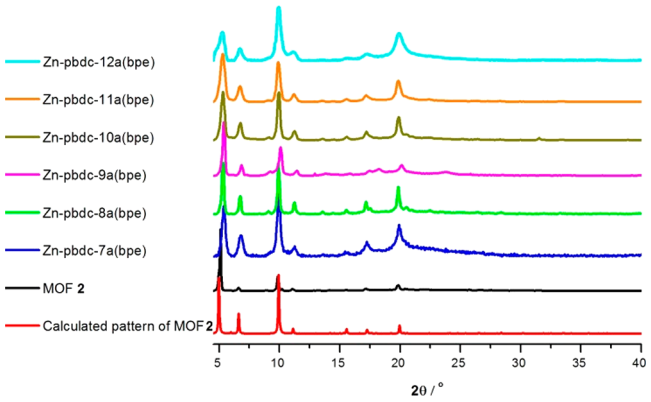

Figure 4. PXRD patterns for Zn-pbdc-7a(bpe), -8a(bpe), -9a(bpe), -10a(bpe), -11a(bpe), -12a(bpe), MOF **2**, and a calculated pattern for MOF **2**.

shown in Figure 4, the majority of Zn-pbdc-*x*a(bpe) particles possess a hexagonal shape on the order of <5 μm, indicating a possible hexagonal crystallization space group.

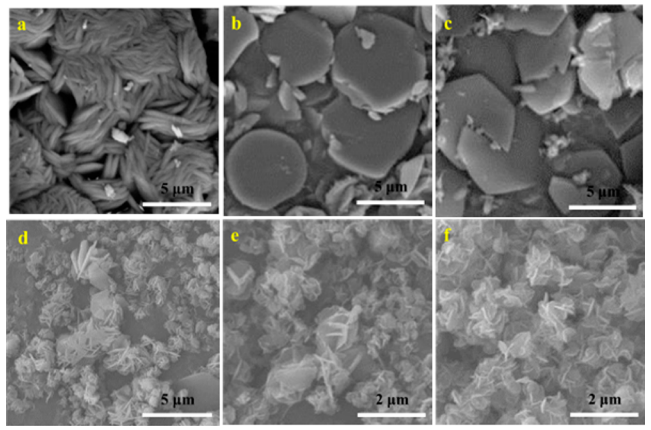

Figure 5. SEM images of Zn-pbdc-7a(bpe) (a), -8a(bpe) (b), -9a(bpe) (c), -10a(bpe) (d), -11a(bpe) (e), and -12a(bpe) (f).

Because the small Zn-pbdc-*x*a(bpe) particles were not suitable for single crystal X-ray diffraction (XRD), we replaced the polymer ligands with a simple H_2bdc ligand to generate an analogous MOF framework (essentially the reverse process used to design the Zn-pbdc-*x*a(bpy) derivatives, Figure 1). BA-bdc (Chart 1) was employed to grow MOF crystals under the same synthesis conditions as Zn-pbdc-*x*a(bpe). Brown block crystals with a formula of $[Zn_7(bdc)_6(H_2O)_6(bpe)_2(NO_3)_2]_n$ (**2**) were harvested. XRD analysis showed that MOF **2** crystallized in the hexagonal $R\bar{3}m$ space group. As shown in Figure 6a, MOF **2** exhibits two kinds of SBUs, a 4-connected $[Zn_2(COO)_3(H_2O)_3N]$ dinuclear SBU and an 8-connected $[Zn_3(COO)_6N_2]$ trinuclear SBU. These two nodes are connected by BA-bdc^{2-} ligands to form a two-dimensional rhombic-grid layer that is further cross-linked by bpe pillars to generate a 4,8-connected fluorite (**flu**) network.[24] Figure 6b shows large free pore spaces in the MOF **2** structure. As shown in Figure 5, the experimental PXRD pattern of Zn-pbdc-*x*a (x = 7–12) fit very well with the calculated pattern of MOF **2** except for the first two peaks are shifted slightly to higher 2θ values. This may be due to slight differences in the unit cells between the polyMOFs and MOF **2**, which could be accommodated as both the polymer ligand and bpe linker are quite flexible.

DOI: 10.1021/jacs.5b11034
J. Am. Chem. Soc. 2016, 138, 920–925

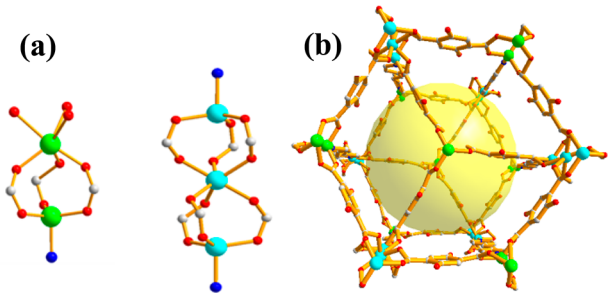

Figure 6. (a) The two types of SBUs in MOF **2** (Zn(II) ions in blue and green); (b) packing diagram of MOF **2** along the *c*-axis direction. The large yellow sphere represents the free pore space in the framework.

To further validate our design methodology, we screened reaction conditions of BA-bdc with "pillaring" pyridine linkers and different metal salts. Using $Cu(NO_3)_2$, a noninterpenetrated, pillared, squared grid MOF **3**, $[Cu_2(BA\text{-}bdc)_2(bpy)]_n$, was obtained.[23] The same reaction conditions using pbdc-8a produced an analogous polyMOF, Cu-pbdc-8a(bpy), which shows the same structure as the parent $[Cu_2(BA\text{-}bdc)_2(bpy)]_n$. Both SEM and PXRD data verified the high crystallinity of Cu-pbdc-8a(bpy) (Figures S18, S19). N_2 sorption data revealed that Cu-bpdc-8a(bpy) is permanently porous and exhibits a BET surface area of 303 ± 32 m^2/g (Figure S20).

To exclude the possibility of polymer ligand degradation during the polyMOF synthesis process, as-synthesized polyMOFs (based on both bpy or bpe) were digested in DMSO-d_6 with the addition of a small amount of concentrated D_2O/DCl. ^{1}H NMR data confirmed that the recovered polymer ligands remained intact (Figures S21−S29). ^{1}H NMR data showed that the ratio of polymer ligand to bpy or bpe was greater than that expected from the known stoichiometry of MOF **1** or **2**. ^{1}H NMR of Zn-pbdc-8a(bpy), -9a(bpy), and -12a(bpy) showed that ratios of pbdc-*x*a (based on the number of bdc units) to bpy are ∼3:1, ∼4:1, and ∼2:1 respectively, while the ratio from the structure of MOF **1** (i.e., based on $[Zn_2(BME\text{-}bdc)_2(bpy)]_n$ and MOF **1**′) should be 2:1. ^{1}H NMR of Zn-pbdc-*x*a(bpe) (*x* = 7−12) showed a ratio of pbdc-*x*a (based on the number of bdc units) to bpe ranging from ∼4:1 to 5:1, while the ratio based on the composition of MOF **2** should be 3:1 ($[Zn_7(BA\text{-}bdc)_6(H_2O)_6(bpe)_2(NO_3)_2]_n$). One possible reason for the apparent excess of polymer in the polyMOFs is that the polymer ligand may create structural defects in the polyMOFs, where the bpy and bpe ligands are absent from some SBUs. Another possibility is perhaps that not all bdc^{2-} groups in pbdc-*x*a ligands can participate in framework formation, resulting in some bdc^{2-} groups from the pbdc-*x*a ligands not being coordinated to the SBUs (i.e., dangling bdc^{2-} ligands within the polyMOFs). It is also possible that polymer ligands extend outside polyMOF crystal domains, serving as coating or binder on the particle surfaces, which perhaps explains the polyMOF films that were observed (Figure 3). Studies are underway to try to distinguish between these different possibilities to understand the discrepancy in the polyMOF stoichiometries.

MOF **1** is reported to have the potential for the capture of CO_2 from flue gases due to its high selectivity for CO_2 vs N_2.[23] Because polyMOFs can adopt the porosity from the parent MOFs, N_2 and CO_2 sorption were examined to evaluate the porosity of the polyMOFs prepared here. The solvent-exchanged polyMOF samples were activated at 130 °C for 10 h under vacuum. As shown in Figure 7a, Zn-pbdc-8a(bpy), -9a(bpy), and -12a(bpy) exhibited type II N_2 sorption

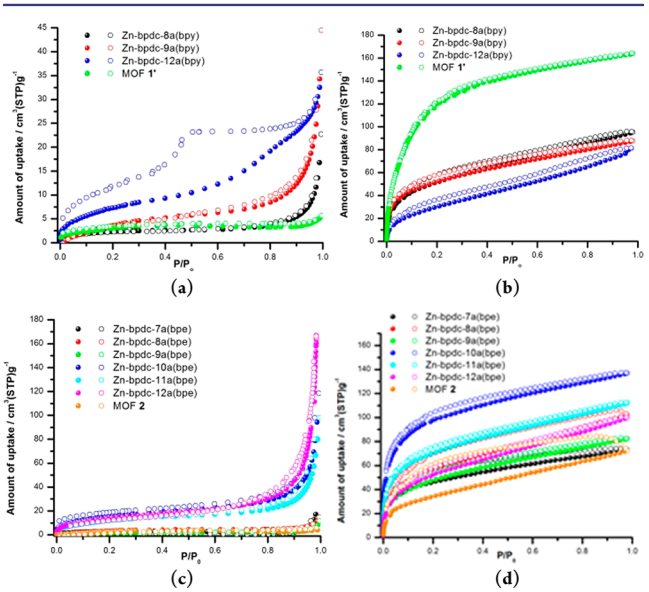

Figure 7. N_2 sorption isotherms at 77 K (a and c) and CO_2 sorption isotherms at 195 K (b and d) for polyMOFs. Closed and open symbols represent the adsorption and desorption isotherms curves, respectively.

isotherms, which are indicative of nonporous or macroporous adsorbents.[25,26] Macroporosity could originate from the packing of the small polyMOF particles (Figure 3). No BET surface areas were calculated based on N_2 sorption due to very low N_2 uptake in the low pressure region of the isotherm. In contrast, Zn-pbdc-8a(bpy), -9a(bpy), and -12a(bpy) were able to absorb 91 ± 5, 86 ± 3, and 75 ± 5 cm^3/g of CO_2, respectively, at 195 K and 1 bar (Figure 7b). A CO_2 uptake capacity of 156 cm^3/g at 195 K and 1 bar was reported for the original MOF **1**,[23] and we determined a CO_2 uptake capacity of 160 ± 6 cm^3/g for MOF **1**′ prepared from BA-bdc (Figure 7b).

As shown in Figure 7c, for MOF **2** type polyMOFs, Zn-pbdc-7a(bpe), -8a(bpe), and -9a(bpe) demonstrated no detectable sorption of N_2 at 77 K in the low pressure region, while Zn-pbdc-10a(bpe), -11a(bpe), and -12a(bpe) exhibited type II N_2 isotherms, again perhaps due to macrovoids between adjacent small particles (particle size <2 μm). For CO_2 sorption, Zn-pbdc-7a(bpe), -8a(bpe), -9a(bpe), -10a(bpe), -11a(bpe), and -12a(bpe) possess CO_2 uptakes of 72 ± 2, 97 ± 5, 80 ± 4, 140 ± 5, 106 ± 5, and 105 ± 6 cm^3/g, respectively, at 195 K and 1 bar (Figure 7d). In contrast, the parent MOF **2** activated under the same conditions as Zn-pbdc-*x*a(bpe) possessed a relatively low CO_2 uptake capacity of 45 ± 5 cm^3/g at 195 K and 1 bar. PXRD revealed that MOF **2** decomposed after activation indicated by the complete disappearance of PXRD peaks after activation (Figure S30). Decreasing the activation temperature to room temperature resulted in an increase of CO_2 uptake to 72 ± 6 cm^3/g for MOF **2** (Figure 7d). However, PXRD analysis revealed that MOF **2** transformed into an unknown crystalline phase after activation even at room temperature (Figure S30).

The observed selective adsorption of polyMOFs can be attributed to a kinetic sieving effect, where the small windows limit the diffusion of larger N_2 molecules (3.64 Å) into pores resulting in reduced adsorption, while smaller CO_2 molecules

DOI: 10.1021/jacs.5b11034
J. Am. Chem. Soc. 2016, 138, 920−925

(3.30 Å) are allowed to enter into the pores of the polyMOFs.[27] This has been observed in several MOFs, which demonstrate selective adsorption for CO_2 over other gases.[28−31] Attempts to quantitatively evaluate the CO_2/N_2 separation performance at 273 and 298 K for these polyMOFs were not successful because N_2 sorption tests were unable to produce smooth isotherm curves due to the extremely low N_2 uptake (e.g., < 1 cm^3/g at 1 bar and 298 K) (Figure S31). Methane uptake was also quite low in these polyMOFs (Figure S31). However, these polyMOFs can absorb significant amounts (11−26 cm^3/g) of CO_2 at 1 bar and 298 K (or 273 K) (Figure S31a, 31b). The zero-coverage isosteric heat (Q_{st}) of CO_2 adsorption for the polyMOFs range from 24.9 to 30.9 kJ/mol (Figure 31c), which are higher than other reported polyMOFs (Zn-bpdc-7a and Zn-bpdc-8a)[11] and some common MOFs such as IRMOF-1, IRMOF-3, and UMCM-1.[32] The conclusion from these measurements is that all tested polyMOFs demonstrate relatively high CO_2 sorption but very low N_2 sorption, making them promising materials for CO_2/N_2 separation, such as those sought in flue gas applications.

Although MOF **1** possesses selectivity for CO_2 vs N_2 and CO_2 vs CH_4, its instability toward water is limiting for real-world applications.[23] Fischer and co-workers reported that MOF **1** transformed to an unknown phase after exposure to a water-saturated atmosphere.[23] Along the same line, we observed that MOF **1′** transformed to a new phase after immersion in water for 1 day at room temperature (Figure S32). Similarly, PXRD revealed that MOF **2** was moisture sensitive and its structure decomposed upon exposure to atmospheric moisture or water for 1 day (Figure S27). As stated earlier, polyMOF variants are expected to have improved water stability compared with their parent MOFs because of polymer hydrophobicity.[11] Contact angle measurements of polymer ligands with water (Table 1) showed that pbdc-9a, -10a, -11a, and -12a were hydrophobic with contact angles of 113 ± 2°, 110 ± 1°, 114 ± 1°, and 120 ± 2°, respectively. Contact angles of the resulting polyMOF samples were also measured to determine if they inherited hydrophobicity from the polymer ligands. Surprisingly, Zn-pbdc-8a(bpy), Zn-pbdc-9a(bpy), Zn-pbdc-7a(bpe), Zn-pbdc-8a(bpe), and Zn-pbdc-9a(bpe) were all relatively hydrophilic, while Zn-pbdc-12a-(bpy), Zn-pbdc-10a(bpe), Zn-pbdc-11a(bpe), and Zn-pbdc-12a(bpe) were hydrophobic with contact angles of 111 ± 1°, 114 ± 1°, 115 ± 1°, and 119 ± 1°, respectively. These findings may best be attributed to the competition between the hydrophobic (e.g., polymer ligand) and hydrophilic (SBU) components of the polyMOFs.

Hydrophobicity alone does not ensure water stability; therefore, PXRD patterns, SEM, and gas sorption experiments were performed for all polyMOFs after exposure to water.[33] PolyMOF samples were immersed in water at room temperature or boiling for 1 day. Water-exposed samples were solvent-exchanged with methanol for 5 days and then activated at 130 °C for 10 h under vacuum. Except for Zn-pbdc-7a(bpe), which lost crystallinity after water treatment, all other polyMOFs retain their crystallinity after water treatment (both room temperature and boiling) as confirmed by PXRD (Figures S33−S41). SEM data revealed all water-treated polyMOFs retained their original morphology, suggesting there was no dissolution or degradation of the original phase (Figures S42−S50). As summarized in Table 2, CO_2 sorption data revealed that Zn-pbdc-11a(bpe), Zn-pbdc-12a(bpe), and Zn-pbdc-12a-(bpy) exhibited very similar CO_2 uptake values before and after water treatment (Figures S51−S53), while the other polyMOF materials lost some porosity after exposure to water (Figures S54−S59). Overall, Zn-pbdc-12a(bpy), Zn-pbdc-11a(bpe), and Zn-pbdc-12a(bpe) show exceptional water stability, while the remaining polyMOFs show significantly improved water resistance compared to their parent materials.

Table 2. Contact Angles and CO_2 Uptake of polyMOFs

polyMOFs	contact angle (deg)	CO_2 uptake (cm^3/g)[a]	CO_2 uptake (cm^3/g)[b]
Zn-pbdc-8a(bpy)	0	91 ± 5	70 ± 5
Zn-pbdc-9a(bpy)	0	86 ± 3	72 ± 4
Zn-pbdc-12a(bpy)	119 ± 1	75 ± 5	78 ± 3
Zn-pbdc-7a(bpe)	0	72 ± 2	40 ± 7
Zn-pbdc-8a(bpe)	0	97 ± 5	70 ± 1
Zn-pbdc-9a(bpe)	0	80 ± 4	61 ± 5
Zn-pbdc-10a(bpe)	111 ± 1	140 ± 5	102 ± 6
Zn-pbdc-11a(bpe)	114 ± 1	106 ± 5	101 ± 5
Zn-pbdc-12a(bpe)	115 ± 1	105 ± 6	106 ± 5
MOF **1**	N/A	156[23]	N/A
MOF **1′**	0	160 ± 6	N/A[c]
MOF **2**	110 ± 1	72 ± 6	N/A[c]

[a]As-synthesized polyMOFs prior to water treatment (195 K and 1 bar). [b]polyMOFs after room temperature water treatment (195 K and 1 bar). [c]CO_2 uptake was not tested because MOF **1′** and MOF **2** are not stable after liquid water treatment.

Because water vapor is a major component of industrial flue gas (~10%), water vapor treatment was also tested to evaluate the stability of Zn-pbdc-12a(bpy), Zn-pbdc-11a(bpe), and Zn-pbdc-12a(bpe), which showed the highest stability to liquid water. PXRD, SEM, and CO_2 sorption data were obtained for these polyMOFs exposed to 90% relative humidity at 25 °C for 7 days. Literature reports indicate that many MOFs, such as HKUST-1 and MOF-74, are not stable under these conditions.[34] Both PXRD and SEM data revealed Zn-pbdc-12a(bpy), Zn-pbdc-11a(bpe), and Zn-pbdc-12a(bpe) retained their crystallinity and original morphology (Figures S37, S38, S41, S46, S47, S50) under the aforementioned conditions. CO_2 sorption data revealed Zn-pbdc-11a(bpe) lost some capacity, giving a lower uptake of 75 cm^3/g at 195 K (Figure S51). Zn-pbdc-12a(bpe) and Zn-pbdc-12a(bpy) exhibited CO_2 uptakes of 98 and 78 cm^3/g, respectively, very close to their uptake values (Table 2) prior to water vapor treatment (Figures S52, S53). For comparison, MOF **1′** and MOF **2** were treated under the same conditions as the aforementioned polyMOFs. PXRD revealed that MOF **1′** retained crystallinity, while MOF **2** did not, further demonstrating the ability of polyMOFs to form analogues of MOFs that are sensitive to either water liquid or vapor.

■ CONCLUSIONS

In summary, we report a mixed ligand strategy, which uses both polymer ligands and simple pillaring pyridine linkers, to prepare new polyMOFs. We also demonstrate that polyMOFs with other metal ions, such as Cu(II), can be prepared, strongly suggesting that our polyMOF approach can be generalized to other metal ions. This finding demonstrates that polyMOFs are compatible with a variety of MOF architectures besides that of the well-studied IRMOF-1. Gas sorption studies revealed that these new materials demonstrated relatively high CO_2 sorption, but very low N_2 uptake, making them promising materials to separate CO_2 from industrial flue gases. Although the parent

DOI: 10.1021/jacs.5b11034
J. Am. Chem. Soc. 2016, 138, 920−925

MOFs are generally unstable to water, the polyMOFs demonstrated excellent water stability. The enhanced water stability is attributed to the incorporation of the hydrophobic polymer ligands, as well as the cross-linking of the MOF lattice by the polymer chains. These findings suggest that polyMOFs may be a general strategy for enabling or improving existing MOFs that need to be made more durable for real-world applications.

■ ASSOCIATED CONTENT

Supporting Information

The Supporting Information is available free of charge on the ACS Publications website at DOI: 10.1021/jacs.5b11034.

Experimental details and additional data (PDF)
Crystallographic data (CIF)

■ AUTHOR INFORMATION

Corresponding Author

*scohen@ucsd.edu

Notes

The authors declare no competing financial interest.

■ ACKNOWLEDGMENTS

This work was supported by a grant from the Department of Energy, Office of Basic Energy Sciences, Division of Materials Science and Engineering under Award No. DE-FG02-08ER46519 (S.M.C.) and the National Science Foundation under Award No. CHE-1305794 (S.A.M.). We also acknowledge the Joint Science and Technology Office for Chemical Biological Defense (JSTO-CBD) for funding under Project Number BA07PRO104.

■ REFERENCES

(1) Beck, J. B.; Rowan, S. J. *J. Am. Chem. Soc.* **2003**, *125*, 13922.
(2) Burnworth, M.; Tang, L.; Kumpfer, J. R.; Duncan, A. J.; Beyer, F. L.; Fiore, G. L.; Rowan, S. J.; Weder, C. *Nature* **2011**, *472*, 334.
(3) Holliday, B. J.; Swager, T. M. *Chem. Commun.* **2005**, 23.
(4) O'Sullivan, T. J.; Djukic, B.; Dube, P. A.; Lemaire, M. T. *Chem. Commun.* **2009**, 1903.
(5) Dobrawa, R.; Lysetska, M.; Ballester, P.; Grüne, M.; Würthner, F. *Macromolecules* **2005**, *38*, 1315.
(6) Dobrawa, R.; Wurthner, F. *Chem. Commun.* **2002**, 1878.
(7) Durkee, D. A.; Eitouni, H. B.; Gomez, E. D.; Ellsworth, M. W.; Bell, A. T.; Balsara, N. P. *Adv. Mater.* **2005**, *17*, 2003.
(8) Foster, J. A.; Parker, R. M.; Belenguer, A. M.; Kishi, N.; Sutton, S.; Abell, C.; Nitschke, J. R. *J. Am. Chem. Soc.* **2015**, *137*, 9722.
(9) Whittell, G. R.; Manners, I. *Adv. Mater.* **2007**, *19*, 3439.
(10) Pawar, G. M.; Lalancette, R. A.; Bonder, E. M.; Sheridan, J. B.; Jäkle, F. *Macromolecules* **2015**, *48*, 6508.
(11) Zhang, Z.; Nguyen, H. T. H.; Miller, S. A.; Cohen, S. M. *Angew. Chem., Int. Ed.* **2015**, *54*, 6152.
(12) Tsotsalas, M.; Liu, J.; Tettmann, B.; Grosjean, S.; Shahnas, A.; Wang, Z.; Azucena, C.; Addicoat, M.; Heine, T.; Lahann, J.; Overhage, J.; Bräse, S.; Gliemann, H.; Wöll, C. *J. Am. Chem. Soc.* **2014**, *136*, 8.
(13) Ishiwata, T.; Furukawa, Y.; Sugikawa, K.; Kokado, K.; Sada, K. *J. Am. Chem. Soc.* **2013**, *135*, 5427.
(14) Furukawa, Y.; Ishiwata, T.; Sugikawa, K.; Kokado, K.; Sada, K. *Angew. Chem., Int. Ed.* **2012**, *51*, 10566.
(15) Distefano, G.; Suzuki, H.; Tsujimoto, M.; Isoda, S.; Bracco, S.; Comotti, A.; Sozzani, P.; Uemura, T.; Kitagawa, S. *Nat. Chem.* **2013**, *5*, 335.
(16) Park, I.-H.; Chanthapally, A.; Zhang, Z.; Lee, S. S.; Zaworotko, M. J.; Vittal, J. J. *Angew. Chem., Int. Ed.* **2014**, *53*, 414.
(17) Uemura, T.; Kaseda, T.; Kitagawa, S. *Chem. Mater.* **2013**, *25*, 3772.
(18) Henke, S.; Schmid, R.; Grunwaldt, J.-D.; Fischer, R. A. *Chem. - Eur. J.* **2010**, *16*, 14296.
(19) Li, H.; Eddaoudi, M.; O'Keeffe, M.; Yaghi, O. M. *Nature* **1999**, *402*, 276.
(20) Choi, E.-Y.; Gao, C.; Lee, H.-J.; Kwon, O. P.; Lee, S.-H. *Chem. Commun.* **2009**, 7563.
(21) Henke, S.; Schneemann, A.; Kapoor, S.; Winter, R.; Fischer, R. A. *J. Mater. Chem.* **2012**, *22*, 909.
(22) Henke, S.; Schneemann, A.; Wütscher, A.; Fischer, R. A. *J. Am. Chem. Soc.* **2012**, *134*, 9464.
(23) Henke, S.; Fischer, R. A. *J. Am. Chem. Soc.* **2011**, *133*, 2064.
(24) Blatov, V. A.; Shevchenko, A. P.; Proserpio, D. M. *Cryst. Growth Des.* **2014**, *14*, 3576.
(25) MacGillivray, L. R. *Metal–Organic Frameworks: Design and Application*; John Wiley & Sons: Hoboken, NJ, 2010.
(26) Zhou, H.-C.; Kitagawa, S. *Chem. Soc. Rev.* **2014**, *43*, 5415.
(27) Li, J.-R.; Sculley, J.; Zhou, H.-C. *Chem. Rev.* **2012**, *112*, 869.
(28) Dybtsev, D. N.; Chun, H.; Yoon, S. H.; Kim, D.; Kim, K. *J. Am. Chem. Soc.* **2004**, *126*, 32.
(29) Pan, L.; Adams, K. M.; Hernandez, H. E.; Wang, X.; Zheng, C.; Hattori, Y.; Kaneko, K. *J. Am. Chem. Soc.* **2003**, *125*, 3062.
(30) Nugent, P.; Belmabkhout, Y.; Burd, S. D.; Cairns, A. J.; Luebke, R.; Forrest, K.; Pham, T.; Ma, S.; Space, B.; Wojtas, L.; Eddaoudi, M.; Zaworotko, M. J. *Nature* **2013**, *495*, 80.
(31) Shekhah, O.; Belmabkhout, Y.; Chen, Z.; Guillerm, V.; Cairns, A.; Adil, K.; Eddaoudi, M. *Nat. Commun.* **2014**, *5*, 4228.
(32) Sumida, K.; Rogow, D. L.; Mason, J. A.; McDonald, T. M.; Bloch, E. D.; Herm, Z. R.; Bae, T.-H.; Long, J. R. *Chem. Rev.* **2012**, *112*, 724.
(33) Burtch, N. C.; Jasuja, H.; Walton, K. S. *Chem. Rev.* **2014**, *114*, 10575.
(34) DeCoste, J. B.; Peterson, G. W.; Schindler, B. J.; Killops, K. L.; Browe, M. A.; Mahle, J. J. *J. Mater. Chem. A* **2013**, *1*, 11922.

DOI: 10.1021/jacs.5b11034
J. Am. Chem. Soc. 2016, 138, 920–925